International Journal of Nanoelectronics and Materials
Volume 15, No. 2, April 2022 [91-106]

Experimental and numerical flexural analysis of porous functionally graded beams reinforced by (Al/Al_2O_3) nanoparticles

Emad Kadum Njim [1*], Sadeq H. Bakhy[1] and Muhannad Al-Waily[3]

[1,2] *Department of Mechanical Engineering, University of Technology, Iraq*
[3]Department of Mechanical Engineering, Faculty of Engineering, University of Kufa, Iraq

Received 10 November 2021, Revised 3 December 2021, Accepted 9 December 2021

ABSTRACT

The porosity distribution, which varies through-thickness direction, plays a vital role in affecting the microstructure and mechanical properties of the final product. This study develops numerical and experimental techniques for the analysis of functionally graded nanobeams with porosity (PFGM). Taking a porous polymeric functionally graded structure as an example, a novel beam can be applied to a broad variety of engineering and biomaterial applications. Tensile specimens were prepared using 3D printing, while flexural bending specimens reinforced with 5% (Al/Al_2O_3) nanomaterial were made using a special system. To study the performance of functionally graded beams with various porosity distributions, numerical solutions were obtained using finite element methods (FEM) and simulations were conducted in ANSYS software. By comparing the obtained results with those obtained from numerical calculations, the experimental solution, including the bending load and midspan deflection, was validated. Additionally, several parameters, such as the porosity parameter, polymer type, and geometrical characteristics, have been studied for their effect on the flexural strength of functionally graded beams. According to the results, it is found that there is a significant effect of the porous parameter and gradient index on the static behavior of functionally graded beams, and nanoparticles enhance bending resistance.

Keywords: FGMs, Flexural analysis, FEA, Nanoparticles

1. INTRODUCTION

The manufacturing of porous functionally graded materials, PFGMs, is generally accomplished using continuous or gradual changes in the porosity distribution [1]. There has been extensive research conducted on the flexural behavior of sandwich structures made of honeycomb, foam, and composite materials [2-3]. The goal of developing FGMs with improved porosity, chemical compositions, and microstructure gradients is to decrease defects due to collisions in structures with composites [4]. On the other hand, FGMs have been applied to multi-layered structures such as laminated or sandwich structures because of the gradual variation of the material properties at the interfaces between the face layers. These structures are usually used in high-temperature environments [5], so it is necessary to have an excellent understanding of the static and dynamic responses of these structures.

The bending problem of functionally graded structures with some important parameters, including volume fraction index, support and loading conditions, and beam configuration, has been studied and introduced in [6] and [7]. These sandwich beams are composed of two isotropic faces and a porous core using different gradients of internal pores. Bending experiments of FGM structures having an exponentially graded core bonded with top and bottom face sheets that are composed of pure ceramic and pure metal, respectively, have also been studied in [8] using the

* Corresponding author: emad.njim@gmail.com

finite element method. Xavior et al. [9] contributed a more detailed experimental study utilizing the tensile, compressive, and 3-point bending flexural test methods to investigate the failure of segmented FG beams made of porous polymer materials. The flexural analysis of composites containing fiber-reinforced syntactic foams has also been investigated [10, 11]. Three-point bending tests and finite element simulations were conducted in parallel to determine the flexural response of the functionally graded polymeric composite beams [12]. Khiloun et al. [13] investigated a numerical model for static and free vibration analysis of the composite structure using a four-variable quasi-3D high deformation shear theory. Yadhav et al. [14] explored the bending behavior of carbon/epoxy composites reinforced with TiO_2 nanoparticles. Seyedkanani et al. [15] conducted different flexural tests on 3D printed samples to examine designs of FGM practicality for improving the characteristics of lightweight structures. The experimental results are verified by finite element analysis.

Koutoati et al. [16] investigated the static and vibration characteristics of the FGM sandwich beam with a porous material, employing shear models and Abaqus software. Hanon et al. [17] studied the mechanical behavior of 3D printed FGM samples consisting of Polytropic acid (PLA) and high-temperature Polytropic acid (HT-PLA). Ghayesh et al. [18] have reviewed the behavior of functionally graded nanoscale and microscale structures. Through the use of nanotechnologies, many different types of nanostructures can be designed, with varied capabilities and purposes. The performance of a nanostructure can be strongly influenced by the surface effect. Consequently, with respect to nanostructures, some researches have recently been conducted using strain gradients, nonlocal stresses, and surface stresses [19, 22]. Gui-Lin She [23] analyzed the mechanical performance of composite nanobeams. The dynamic and thermal behavior of porous FG nanobeams has been studied using the nonlocal finite element method and shear deformation theory [24, 25]. The literature reveals that there were very limited studies conducted on the flexural analysis of porous nanobeams, and most of the researchers incorporated only the numerical and analytical results without considering the experimental work with porous polymer FG beams.

The prime aim of this study is to investigate the influence of porosity material gradation and nanomaterial on the bending behavior of porous FG beams having a variation in stiffness through thickness using flexural analysis of a novel functionally graded porous polymer beam. A mathematical model to calculate the beam flexural stiffness, the maximum bending strength load, and the deflections when tested on flat beams with porosities was developed using various parameters (porosity parameter, power-law index, and nanoparticles). The finite element method (FEM) was used to verify the experimental results. This paper is arranged as follows: Section 2 introduces a theoretical investigation of the FG structure. FEA is described in Section 3 as a mean of verifying calculations. Section 4 presents the results, with helpful discussions, of the flexural test of the imperfect FG beam. Section 5 of this paper contains some crucial conclusions that are related to the flexural behavior of FG beams with an even distribution of porosities and effective suggestions for future work.

2. MATERIAL AND METHODS

In this work, Polylactic Acid (PLA) samples widely used in industrial applications are incorporated. The raw materials were supplied from the international market (China) and designed for tensile and bending tests. For each test, two kind of products were fabricated, one with a homogeneous density and the other with a varied density along with its thickness. Aluminum Oxide Nanoparticles of Al_2O_3 with various percentages were used for both homogenous and porous polymers.

2.1 The Analytical FGM Beam Model

Generally, an FGM beam is made of two distinct constituents, such as ceramic and metal, which were commonly considered in most of the previous works found in the literature. As shown in Figure 1, for a beam with length (L) and thickness (h), the top surface is assumed to be ceramic-rich ($z = h/2$) and gradually varies to the bottom surface ($z = -h/2$). Due to defects in the manufacture of FGM beams, the porosity distribution would be even across the beam thickness. Thus, by introducing a power-law distribution scheme, the volume fraction of the upper constituent could then be assumed to be in the form of [26],

$$V_1(z) = \left(\frac{z+\frac{h}{2}}{h}\right)^g \tag{1}$$

The corresponding volume fractions of the mixture can be given by,

$$V_1(z) + V_2(z) = 1 \tag{2}$$

where V_1 denotes the upper surface volume fraction and V_2 denotes the lower surface volume fraction; g denotes a power-law variation index ($g \leq 0 \leq \infty$) that describes material property variation in thickness. The effective material properties of the FG beam can be formulated as,

$$P(z) = (P_1 - P_2)\left(\frac{z+\frac{h}{2}}{h}\right)^g + P_2 \tag{3}$$

In Equation (3), P_1 and P_2 are the corresponding material properties of the upper and lower constituents of the FG beam, respectively. Poisson's ratio is assumed to be constant over the thickness and is equal to 0.4 throughout the paper [26]. The novel FG beam is assumed in the current study to be composed of only one metal with an equal distribution of the porosity volume fraction (1) and to be graded through-beam thickness. Hence, the suggested rule for the volume fraction according to the power-law function is as follows [27],

$$V_p(z) = V_m - \alpha . V_m \left(\frac{z}{h} + \frac{1}{2}\right)^g \tag{4}$$

For example, $g = 0$, $V_p\,(z) = V_m - \alpha\, V_m$, while $g = \infty$, $V_p = V_m = 1$, where V_p is the total volume of porous metal, V_m is the volume of core metal, and α is the porosity parameter. Consequently, the proposed mechanical properties of the FGM porous metal can be represented as,

$$P(z) = P_m - \alpha . P_m \left(\frac{z}{h} + \frac{1}{2}\right)^g \tag{5}$$

Here, P_m is the value of the material properties of metal of the FG beam. Thus, for the homogenous beam (α = 0), while for the imperfect FG beam, the material properties: Young's modulus (E) and mass density (ρ) of the FG beam can be expressed as,

$$E(z) = E_m - E_m \alpha \left(\frac{z}{h} + \frac{1}{2}\right)^g \tag{6}$$

$$\rho(z) = \rho_m - \rho_m \alpha \left(\frac{z}{h} + \frac{1}{2}\right)^g \tag{7}$$

In a 3-point bending test, the total deformation (δ) due to bending and shear at the beam midspan may be obtained by using the following equation [28],

$$\delta = \delta_b + \delta_s = \frac{Fl^3}{48(EI)_{eq.}} + \frac{Fl}{4(AG)_{eq.}} \quad (8)$$

where F is the bending load, l (span), A is the area of the beam's cross-section, and G(modulus of shear). So, the overall stiffness of both of these components will be,

$$(EI)_{eq.} = \left(\sum E_i \left(\frac{b\, {h_i}^3}{12} + (bh_i)\, {h_i}^2\right)\right) \quad (9)$$

Moreover, the equivalent shear rigidity ($AG_{eq.}$) becomes,

$$(AG)_{eq.} = bhG_{eq.} \quad (10)$$

The subscripts h and b refer to the beam thickness and the width, respectively. The beam's effective shear modulus ($G_{eq.}$) can be obtained as,

$$G_{eq.} = \frac{E_{eq.}}{2(1+\nu)} \quad (11)$$

$$E_{eq.} = E(z) = E_m - E_m \alpha \left(\frac{z}{h} + \frac{1}{2}\right)^g \quad (12)$$

The flexural stress σ_f for a rectangular cross-section can be calculated as,

$$\sigma_f = \frac{3FL}{2bh^2} \quad (13)$$

Additionally, the value of dissipated strain energy S is equal to,

$$S = \frac{M^2}{2b(EI)_{eq.}} \quad (14)$$

where the maximum bending moment M is calculated as,

$$M = \frac{Fl}{4} \quad (15)$$

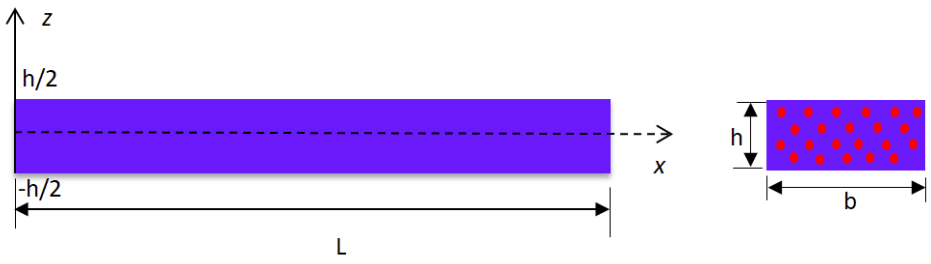

Figure 1. The geometry of the FGM beam with porous distribution through-beam thickness

2.2 Experimental work

2.2.1 Sample Preparation

The following schematic shows the process of fabricating porous FG samples reinforced with aluminum oxide nanoparticles (Al_2O_3). Samples for each test were prepared following standard specifications. Firstly, the polymer wire with a diameter of 1.75 mm was used as raw material, which was fed into the stainless steel cone of the plastic lab mini laboratory SJ25 solo screw extruder extrusion machine. Next, nanoparticles of Al_2O_3 are weighted on a precision scale and fed into the extruder for mixing with polymer wire. With adequate time and temperature, the flow of polymer through the extruder barrel and mold generated by the extruder head produces a wire nano polymer with appropriate dimensions and properties. A micrometer is used to measure the diameter with precision (0.001). Lastly, a new wire is used in 3D printing machines of type CR-10 MAX. The tested samples were designed by using the Solid Works program, saving the geometry as a (.stl) file, and then using the 3D printer to produce the final form of the samples. Figure 2 shows the processing procedure of Nano PFGM beams.

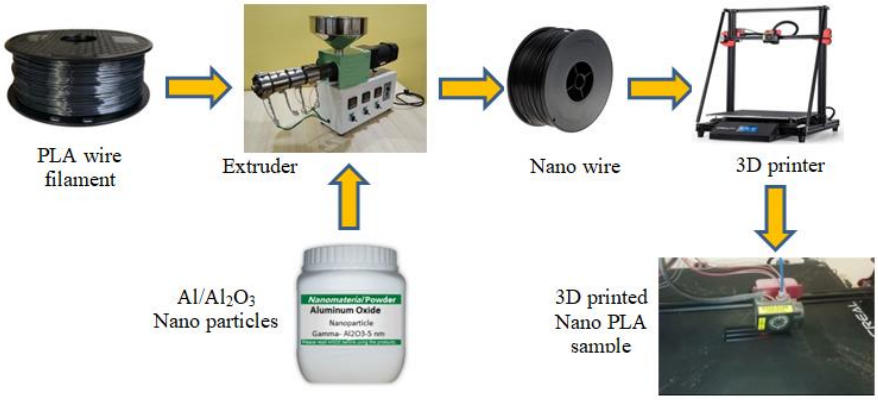

Figure 2. Flow chart of fabrication Nano PFGM beams

2.2.2 Tensile Test

Tensile properties are used to select different materials. To ensure quality, materials are often tested to determine if their tensile properties comply with the requirements specified in their specifications. Figure 3(a) illustrates the photo geometry and specimen dimensions. According to ASTM standard D638 [29], polymer samples (see Figure 3(b)) were produced through 3D printing. A microcomputer-controlled universal testing machine (UTM) type (Tinius Olsen H50KT) is used to perform uniaxial tensile tests. Tensile strength has been limited for the polymer samples. The results of the stress-strain measurements of the 3D-printed samples subjected to tensile loading are shown in Figure 4. Table 1 also records the average of six readings for the PLA sample as an additional measurement of accuracy.

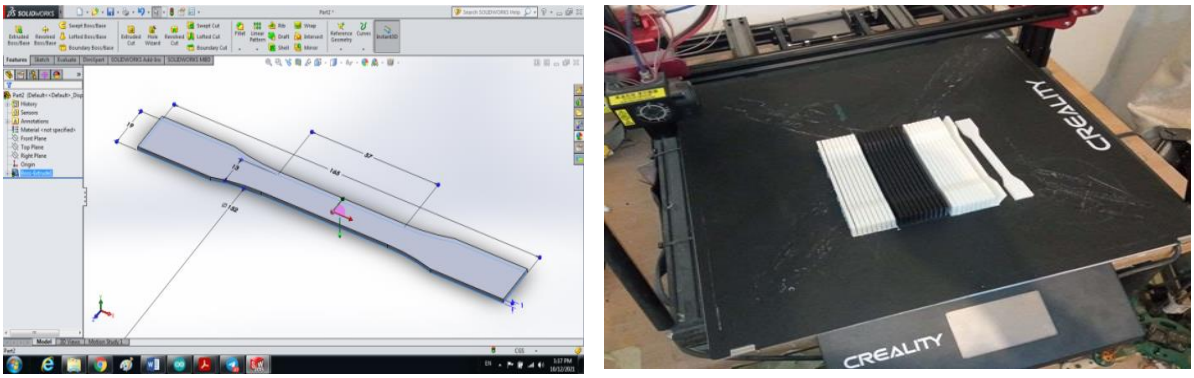

(a) (b)

Figure 3. (a) A schematic diagram of the tensile specimen (mm) according to ASTM standard D3763, (b) 3D printed polymer tensile test samples

.

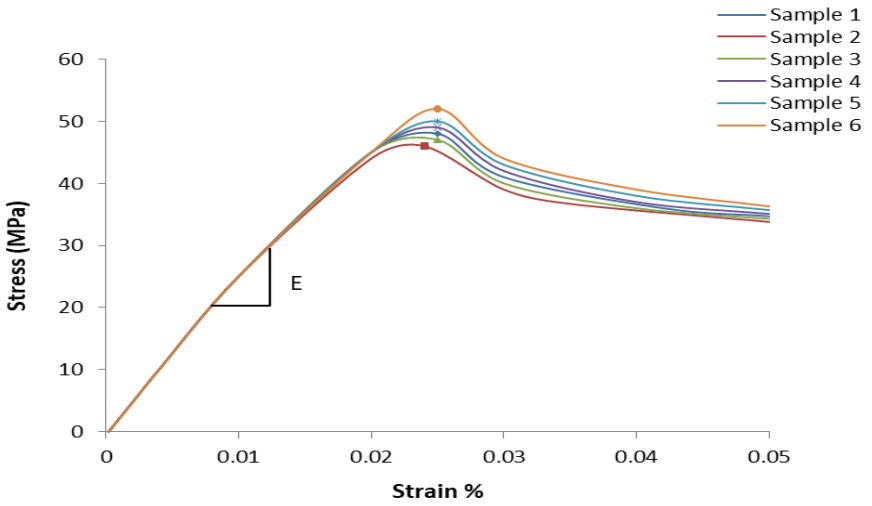

Figure 4. Stress-strain curves of PLA samples under tensile load

Table 1. Averaged experimental mechanical properties of PLA samples

Young's modulus (GPa)	Ultimate strength (Mpa)	Ultimate strain
2.2∓ 0.1	46.5 ∓1.25	0.025 ∓ 0.0014

2.2.3 Three-point bending test

This study aims to design and generate a porosity distribution pattern for functionally graded cores. Typically, this arrangement follows the power-law distribution of the volume fraction of the pore area. 3D printing is an increasingly popular manufacturing technology that involves generating 3D models of a product using CAD software or by scanning an existing object [30]. Metallic ropes or filaments are melted inside the printer's head during this process. The wire is passed through the nozzle, which discharges the molten batch. During the feeding process, continuous layers of material are deposited into a molten state to form objects. The workpiece is mounted on a bench that moves downward in a z-direction. In other words, it will create a 3D entity that is accurately the same as the designed model after a certain period. Among the most commonly used materials for 3D printing is PLA, which is a major source and is perfect for most industrial, medical, and household applications [31]. Polymer specimens with porosity were made in local markets according to ASTM standard D790 [32]. Table 2 shows the geometrical properties of beam samples used in experiments.

The three-point bending test is often used to evaluate the bending performance of sandwich panels and study their impact resistance. This is used to determine the sandwich flexural strength, stiffness, and core shear modulus of all types of materials and structures. According to standard recommendations, a roller with a diameter of 10 mm applies the load to a sample that is supported by two rollers, each with a diameter of 10 mm. A simply supported rig is used to maintain the crosshead speed of 4 mm/sec. A transducer, deflectometer, or dial gauge can be used to measure the midspan deflection. By applying the load at the center of the specimen, the displacement was recorded on a PC; hence, load-deflection curves can be generated to determine the sandwich stiffness and core shear modulus. Three-point bending was used to measure at least five (5) FG

samples, with a total of fifteen (15) for each porosity parameter value. Figure 5 depicts the three-point bending test schematic, while Figure 6 shows the experimental setup for the FG beam.

Table 2. The dimensions of PLA specimens used

Porosity	Power-law Index	Dimensions (mm)	Thickness (mm)
0	0.5	60 x 10	6
0	1	60 x 10	6
0	2	60 x 10	6
0.1	0.5	60 x 10	6
0.1	1	60 x 10	6
0.1	2	60 x 10	6
0.2	0.5	60 x 10	6
0.2	1	60 x 10	6
0.2	2	60 x 10	6
0.3	0.5	60 x 10	6

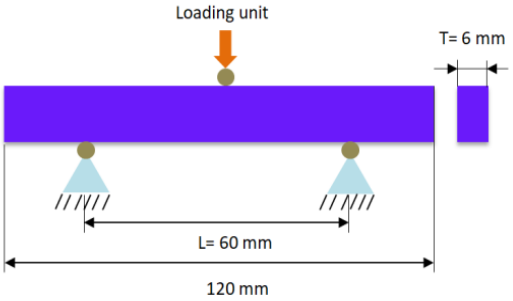

Figure 5. Three-point bending test configuration

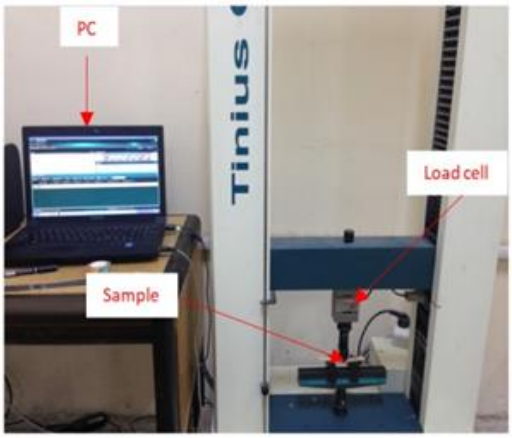

Figure 6. Experimental setup for the FG beam

3. FINITE ELEMENT ANALYSIS

Finite Element Modeling (FEM) is carried out to check the accuracy of numerical results with those obtained throughout three-point bending experiments [33–35]. In this work, the commercial ANSYS software program 2021 R1 was executed to analyze the bending analysis of the sandwich beam. The beam model is generated, employing the SHELL99 composite element type as shown in Figure 7. A convergence mesh study was carried out and the corresponding boundary conditions for the model were applied. Load is applied gradually and simply supported boundary conditions are used as shown in Figure 8. In order to provide more details about the behavior of various porous materials, three types of polymers were employed: thermoplastic polyamide elastomer (TPU), Polyetheretherketone (PEEK), and Acrylonitrile Butadiene Styrene (ABS). The material characteristics used in the FE simulation are calculated using Equations (6–8) and then introduced into the engineering library view of ANSYS. The general mechanical properties of PLA were used according to the results of the experimental work (Table 2), while

the other three polymer types were given in Table 3 [36]. Based on various parameters, the bending load, total deformation, strain energy, and midspan deflection of the PFGM beam are analyzed under static structural analysis. In addition, the flexural strength and energy absorption of the FG beam are calculated using three porosity coefficients (α = 10%, 20%, and 30%), a gradient exponent (g = 1 to 25), and various beam thicknesses (5–20 mm).

Table 3. Mechanical properties of materials used [36]

Property	TPU	PEEK	ABS
Modulus of elasticity (GPa)	0.8	7.7	2.5
Mass density (kg/m^3)	1360	1410	1425
Poisson's ratio	0.4	0.4	0.4

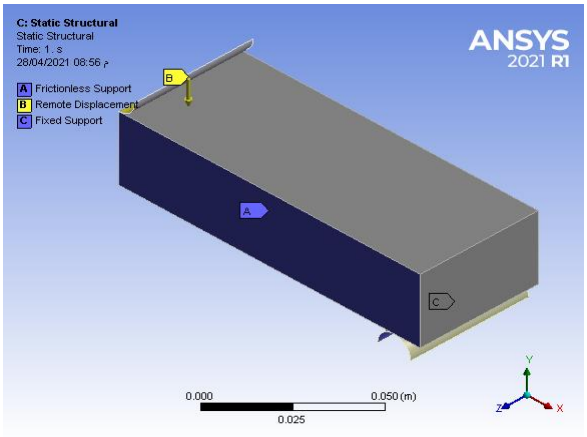

Figure 7. A 3D model of the FG beam with BCs

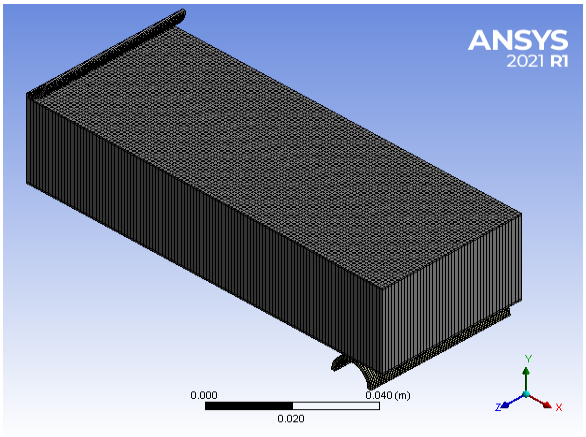

Figure 8. A 3D model with a mesh

4. RESULTS

The influence of porosity parameters, beam thickness, and nanoparticles on the static behavior of porous polymer FG beams is examined in this section. The FG beam dimensions were made according to the ASTM D790 standard [32] (i.e, L = 60 mm, W = 10 mm), while the beam height was h = 5 – 20 mm. A universal testing machine (Tinius Olsen H50KT apparatus) was used to examine samples with three porosity parameters (α = 0.1, 0.2, and 0.3) and a gradient index (g = 0.5, 1, 2). The experimental results including the maximum bending load and maximum total deflection at the mid-span of beams were obtained by utilizing the PC of the testing instrument. The experimental results of the load-displacement curves for simply supported PFGM beams at porosity (α=0.2), power-law index (g=1), and beam thickness of 6 mm are shown in Figures 9 and 10. According to the results, the nanoparticle reinforced FG beam exhibits improved bending strength. Tables 4-7 present the validation of results due to experiments using the ANSYS software 2021 R1. According to the findings in Tables (4 and 5), one can see that the value of the maximum bending load decreases with increasing values of the porosity parameter. The maximum difference between experimental and numerical bending load results is 10%. The influence of adding 5% (Al/Al_2O_3) nanoparticles enhanced the bending strength by 10%.

On the other hand, Tables 6 and 7 presented experimental and numerical results of maximum deflection occurring at the beam midspan with and without using nanoparticles. Based on the

obtained numerical results, it is observed that the maximum difference in deflection between experimental and ANSYS simulation does not exceed 10%. For the same FG beam geometrical properties, this percentage is influenced by the power-law index and porous factor. It can be concluded that the maximum deflection decreases with increasing porosity factor due to the decrease in material rigidity. Similarly, the use of nanoparticles strengthened the beam resistance towards deformation. One potential source of error is that the mechanical properties formula used was based on the classical beam theory (CBT), whereas the FEA solution was obtained using the assumption of the first-order shear deformation beam theory (FSDT). In addition, noise and system errors also determine the accuracy and reliability of the experimental static analysis. However, the most significant observations noticed from the configuration of defective specimens throughout the experiments are that the most common reason for failure observed in the beam was the beam yielding, as well as the possible deformation of the beam due to shear, which will initiate and develop at the PLA layers with a high porosity ratio.

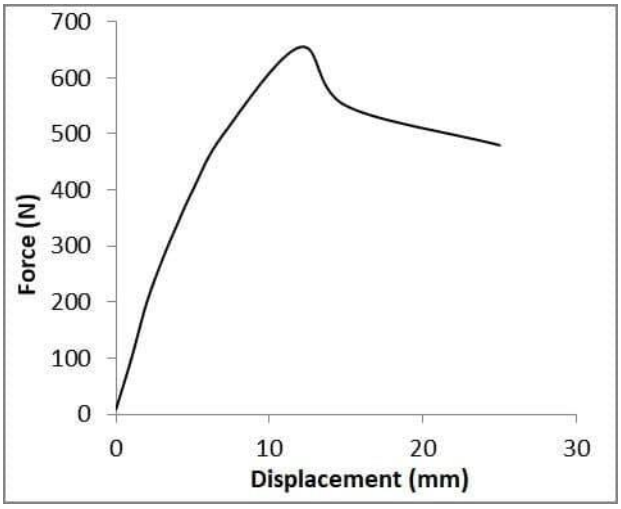

Figure 9. The experimental force-displacement curve without nanoparticles at porosity (α = 0.2) and gradient index (g = 1)

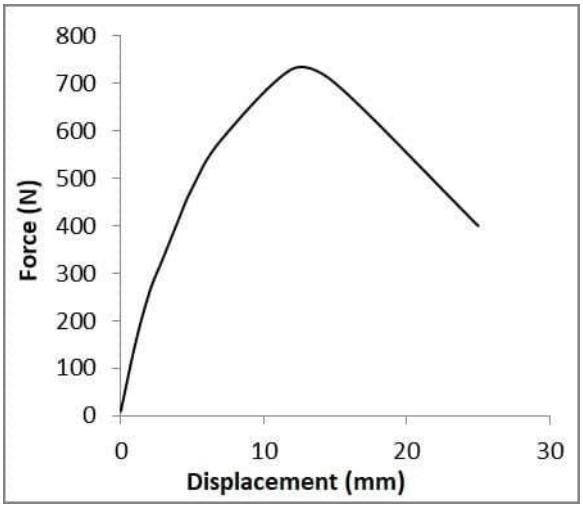

Figure 10. The experimental force-displacement curve with nanoparticles at porosity (α = 0.2) and gradient index (g = 1)

Table 4. The numerical and experimental maximum bending load (N) without nanoparticles

Alpha	*g*	Thickness (mm)	Exp.	Num.	Discrepancy %
0	0.5	6	273	280	5.536
0	1	6	840	866	6.250
0	2	6	1600	1725	7.246
0.1	0.5	6	185	199	7.035
0.1	1	6	705	767	8.083
0.1	2	6	1250	1375	9.091
0.2	0.5	6	165	184	9.341
0.2	1	6	655	688	5.072
0.2	2	6	1180	1288	8.385
0.3	0.5	6	148	166	9.639
0.3	1	6	590	645	8.527
0.3	2	6	1100	1255	10.057

Table 5. The numerical and experimental maximum bending load (N) with nanoparticles (5% Al/Al_2O_3)

Alpha	*g*	Thickness (mm)	Exp.	Num.	Discrepancy %
0	0.5	6	303.03	326.79	7.271
0	1	6	930.4	990.56	6.073
0	2	6	1770	1919.75	7.800
0.1	0.5	6	209.35	222	5.698
0.1	1	6	788.55	855	7.772
0.1	2	6	1380.5	1530	9.771
0.2	0.5	6	187.15	200	6.425
0.2	1	6	737.05	777	5.142
0.2	2	6	1304.8	1435	9.073
0.3	0.5	6	162.5	180	9.722
0.3	1	6	657.9	711	7.468
0.3	2	6	1219	1357.53	10.205

Table 6. The numerical and experimental maximum bending deflection without nanoparticles (mm)

Alpha	*g*	Thickness (mm)	Exp.	Num.	Discrepancy %
0	0.5	6	11	11.8	6.780
0	1	6	9.8	10.35	5.3
0	2	6	8.75	9.38	6.7
0.1	0.5	6	13.5	14.7	8.163
0.1	1	6	11.8	12.85	8.171
0.1	2	6	9.56	10.44	8.429
0.2	0.5	6	14.2	15.35	7.492
0.2	1	6	12.75	13.65	6.593
0.2	2	6	10.48	11.5	8.870
0.3	0.5	6	15.67	16.85	7.003
0.3	1	6	13.9	14.75	5.763
0.3	2	6	9.85	10.64	7.425

Table 7. The numerical and experimental maximum bending deflection with nanoparticles (mm) (5% Al/Al_2O_3)

Alpha	*g*	Thickness (mm)	Exp.	Num.	Discrepancy %
0	0.5	6	12.17	13.25	8.151
0	1	6	10.5	11.4	7.9
0	2	6	9.6	10.65	9.859
0.1	0.5	6	14.8	16.35	9.480
0.1	1	6	13.2	14.5	8.966
0.1	2	6	10.35	11.45	9.607
0.2	0.5	6	15.5	16.9	8.284
0.2	1	6	14.2	15.35	7.492
0.2	2	6	11.4	12.45	8.434
0.3	0.5	6	17.1	18.5	7.568
0.3	1	6	15.2	16.2	6.173

0.3	2	6	10.5	11.4	7.895

For better understanding, the following dimensionless relation was used to define the deflection parameter [37],

$$\bar{w} = \frac{100 E_m b h^3}{F l^3} . w\,(x, z) \tag{16}$$

where $\bar{w}$ is the deflection parameter, E_m is the elastic modulus of the beam metal, and w (x, z) is the maximum deflection.

Figures (11–14) show the 3D surface generated by the MATLAB environment in terms of non-dimensional deflection parameters as a function of gradient indices and beam thickness of a simply-supported FG beam with a PLA core. The results show that the deflection parameter increases with both the porosity ratio and power-law index. The variation in results increases positively with the increase of the volume fraction exponent. This indicates that the beam exhibits more ductility.

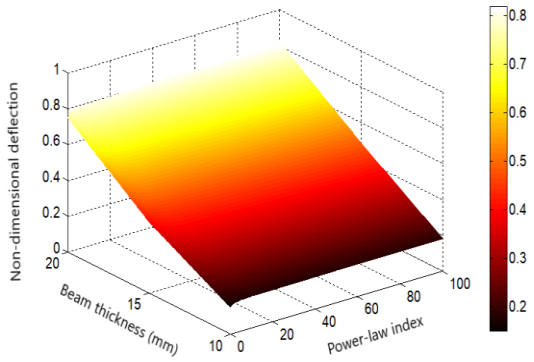

Figure 11. 3D surface plot of the simply supported sandwich beam at porosity (α=0.1) without nanoparticles

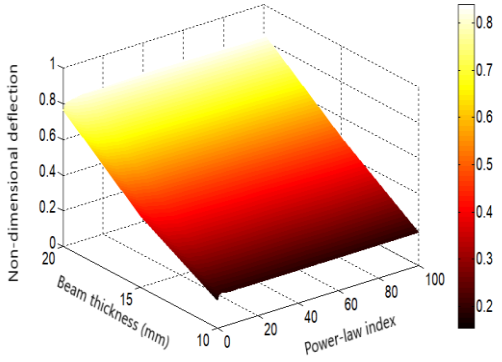

Figure 12. 3D surface plot of the simply supported sandwich beam at porosity (α=0.1) with nanoparticles (5% Al/Al_2O_3)

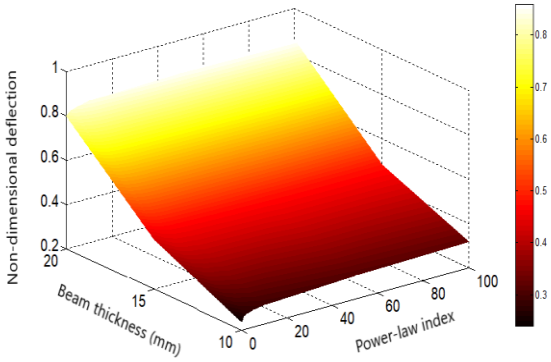

Figure 13. 3D surface plot of the simply supported sandwich beam at porosity (α=0.2) without nanoparticles

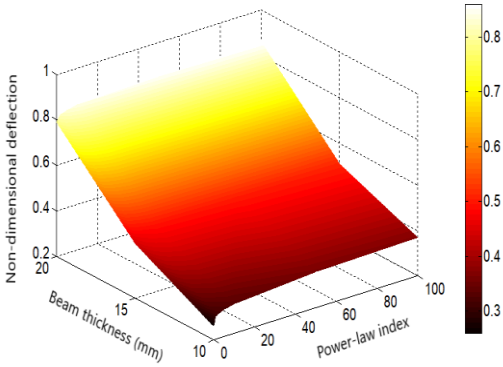

Figure 14. 3D surface plot of the simply supported sandwich beam at porosity (α=0.2) with nanoparticles (5% Al/Al_2O_3)

Figure 15 gives the numerical results of the strain energy of a simply-supported porous PLA beam without reinforcement by nanoparticles, with various porosity factors (α= 0.1, 0.2, and 0.3), a beam thickness of 6 mm, and by using six values of volume fraction index (g = 0.5, 1, 2, 5, 10, and 25). Because of the decrease in material toughness, the strain energy decreases with increasing porosity parameters and gradient index. On the other hand, Figure 16 shows the same configuration using nanoparticles. From those figures, one can conclude the influence of

nanoparticles on the enhancement strength of FG beams. Figures (17 and 18) show the SEM micrographs of the fractured surface of a graded sample using backscattered electrons (BSE) and secondary electrons (SE) on the 250 W laser power region at a porosity parameter (0.1) without and with reinforced nanoparticles of Al/Al_2O_3, respectively, at a beam thickness of 6 mm, using various working distances (WD) for each sample. No striations were found on fractured surfaces. However, they can be seen in the grain boundaries with different local orientations in adjacent grains or melt pool boundaries. Figure 19 shows numerical results performed by ANSYS of maximum bending load at power-law index (g = 0.5) and beam thickness of 10 mm using various polymer beam metals. In the same fashion, the deflection parameter results are shown in Figure 20. From the results, it can be concluded that the beam made of PEEK exhibits more deflection than ABS and TPU, respectively. Furthermore, as the porosity ratio increases gradually, the deflection values decrease because the material stiffness decreases.

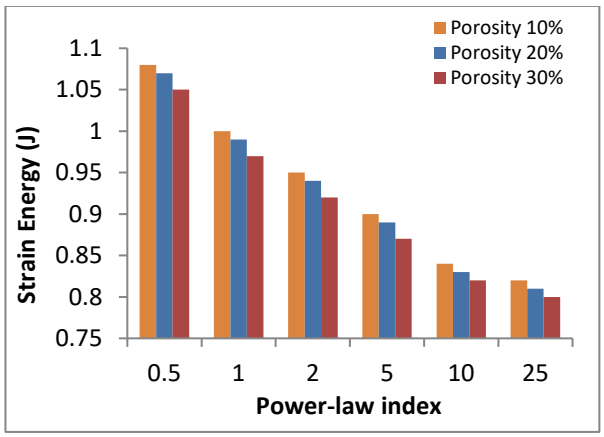

Figure 15. The strain energy of a simply-supported beam at various volume fraction indices without nanoparticles

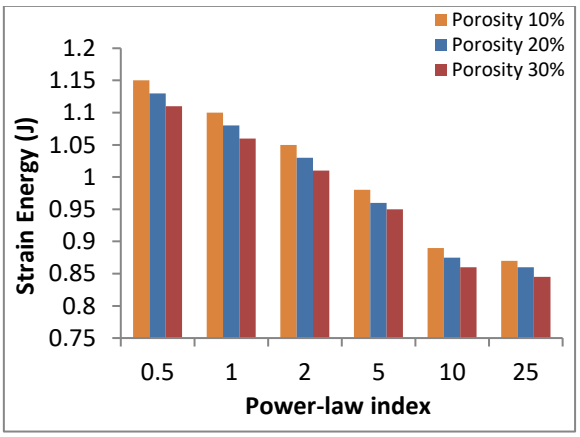

Figure 16. The strain energy of a simply-supported beam at various volume fraction indices with nanoparticles (5% Al/Al_2O_3)

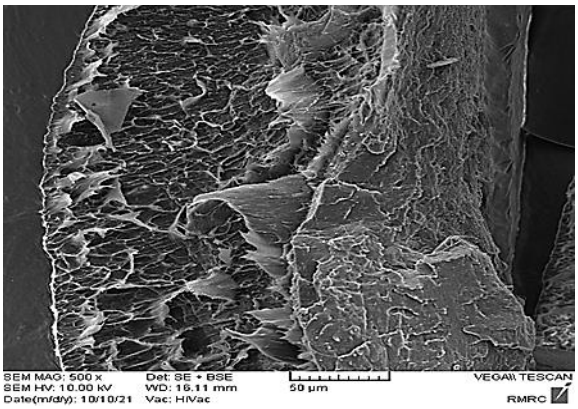

Figure 17. Sem images for PLA samples with a porosity of 0.1 and without nanoparticles

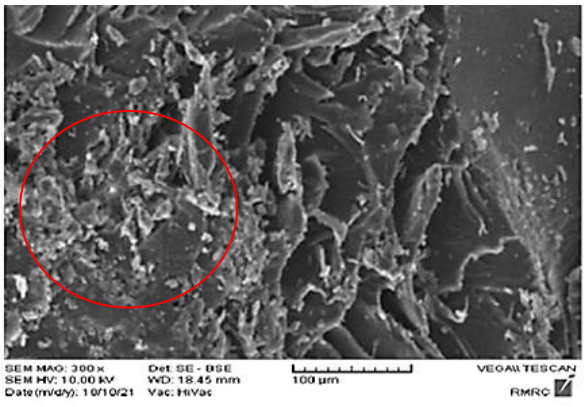

Figure 18. Sem images for PLA samples with porosity of 0.1 and 5% Al/Al_2O_3 nanoparticles

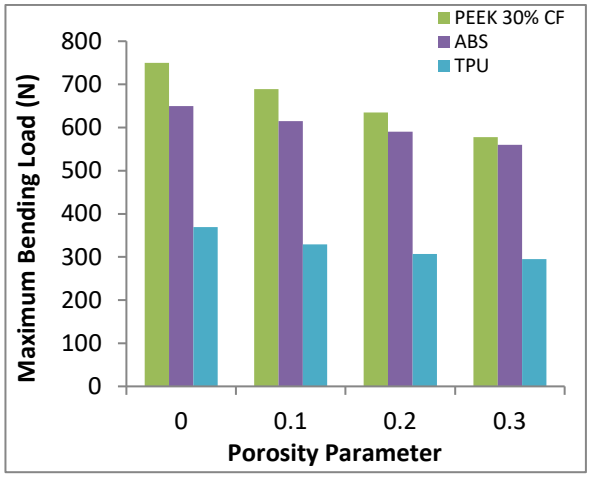

Figure 19. Maximum bending load for various metal types at g = 0.5, beam thickness of 10mm

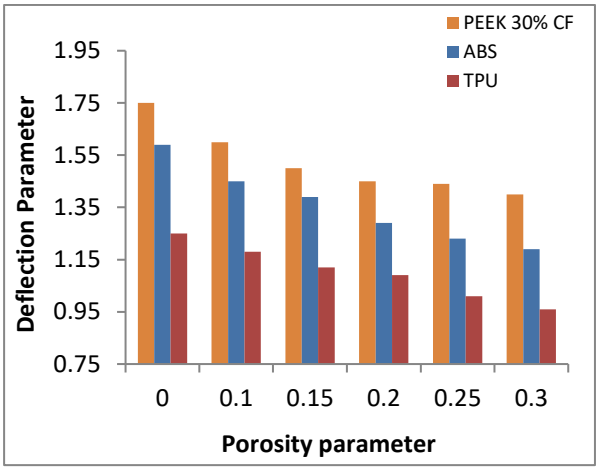

Figure 20. Variation of deflection parameters for g = 0.5 and beam thickness of 10mm

5. CONCLUSIONS

This paper examines the flexural strength and stiffness of porous functionally graded beams. This contribution also relates to the combined numerical design and experiment of the PFGM sandwich structure. The results showed that the experimental bending loads can be increased by the addition of (Al/Al_2O_3) nanoparticles. The increase will be 9.9% as a result of reinforcement by nanoparticles at porosity 0 and a power-law index (g = 0.5), while at the same gradient index but at porosity 0.3, the increase will be 8.93%. In addition, the FG beams show a noticeable reduction in bending stiffness and ultimate load due to the decrease in porosity. When the porosity coefficient decreases, both bending stiffness, and mid-span displacement increase. A fair convergence between both experimental and ANSYS analysis, where the maximum error percentage is found to be no more than 10% in bending and 9% in deflection measurement, which indicates that a 3D printing method can be used to manufacture good PFGM samples. Designing and optimizing functionally graded beams requires the use of numerical and experimental methods.

REFERENCES

[1] Emad, K., N., Bakhy, H., S., and Al-Waily, M., A Review of the Recent Research on the Experimental Tests of Functionally Graded Sandwich Panels, Journal of Mechanical Engineering Research and Developments. 44, 3 (2021) pp. 420-441.

[2] A., Garg, M., O., Belarbi, H., D., Chalak, A., Chakrabarti, A review of the analysis of sandwich FGM structures, Composite Structures. 258 (2021).

[3] Ghatage, P., S., Kar, V., R., Sudhagar, P., E., On the numerical modelling and analysis of multi-directional functionally graded composite structures: a review. Compos. Struct. 236 (2020).

[4] Emad, K., N., Bakhy, H., S., and Al-Waily, M., Analytical and Numerical Investigation of Buckling Behavior of Functionally Graded Sandwich Plate with Porous Core, Journal of Applied Science and Engineering. 25, 2 (2022) pp. 339-347.

[5] S., E., Sadiq, M., J., Jweeg, and S., H., Bakhy, Strength analysis of aircraft sandwich structure with a honeycomb core: Theoretical and Experimental Approaches, Engineering and Technology Journal. 39/1 (2021)153-166.

[6] A., Karakoti, S., Pandey, and V., R., Kar, Bending analysis of sandwich shell panels with exponentially graded core, Materials Today: Proceedings 28, 3 (2020) 1706-1708.

[7] M., A., Hamed, R., M., Abo-bakr, S., A., Mohamed, and M., A., Eltaher, Influence of axial load function and optimization on static stability of sandwich functionally graded beams with porous core, Eng. Comput., 36 (2020) 1929–1946.

[8] M., A., Xavior, D., Nishanth, N., N., Kumar, and P., Jeyapandiarajan, Synthesis and Testing of FGM made of ABS Plastic Material, Materials Today: Proceedings. 22, 4 (2020) pp. 1838-1844.

[9] Z., Huang, Y., Zhou, G., Hu, W., Deng, H., Gao, and L., Sui, Flexural resistance and deformation behavior of CFRP-ULCC-steel sandwich composite structures, Composite Structures. 257 (2021).

[10] M., Kazemi, Experimental analysis of sandwich composite beams under three-point bending with an emphasis on the layering effects of foam core. 29 (2021) 383-391.

[11] A., A., Daikh and A., M., Zenkour, Effect of porosity on the bending analysis of various functionally graded sandwich plates, Materials Research Express. 6, 6 (2019).

[12] Garg, H., D., Chalak, and A., Chakrabarti, Comparative study on the bending of sandwich FGM beams made up of different material variation laws using refined layerwise theory, Mechanics of Material. 151(2020).

[13] M., Khiloun, A., A., Bousahla, A., Kaci, A., Bessaim, A. Tounsi, and S.R. Mahmoud, Analytical modeling of bending and vibration of thick advanced composite plates using a four-variable quasi 3D HSDT. Engineering with Computers. 36, 3 (2020) pp. 807-821

[14] B., R., L., Yadhav, H., K., Govindaraju, M., D., Kiran, B., Suresha, Three-point bending and impact behavior of carbon/epoxy composites modified with titanium dioxide nanoparticles, Materials Today: Proceedings. (2020).

[15] Seyedkanani, H. Niknam, and A. H. Akbarzadeh, "Bending behavior of optimally graded 3D printed cellular beams," Additive Manufacturing. 35 (2020).

[16] K., Koutoati, F., Mohri, E., Daya, and E., Carrera. A finite element approach for the static and vibration analyses of functionally graded material viscoelastic sandwich beams with nonlinear material behavior, Composite Structures. 274 (2021).

[17] M., M., Hanon, R., Marczis, and L., Zsidai, Influence of the 3D Printing Process Settings on Tensile Strength of PLA and HT-PLA, Periodica Polytechnica Mechanical Engineering. 65, 1 (2021) pp. 38–46.

[18] Ghayesh, M., H., and Farajpour, A., A review on the mechanics of functionally graded nanoscale and microscale structures. Int. J. Eng. Sci. 137 (2019) pp. 8–36.

[19] Chinika D., Roshan L., and Sukavanam N., Effect of surface stresses on the dynamic behavior of bi-directional functionally graded nonlocal strain gradient nanobeams via generalized differential quadrature rule, European Journal of Mechanics - A/Solids. 90. (2021).

[20] Lal, R., and Dangi, C., Dynamic Analysis of Bi-directional Functionally Graded Timoshenko Nanobeam based on Eringen's Nonlocal Theory Incorporating the Surface Effect. 395 (2021a).

[21] Rahmani, A., Faroughi, S., Friswell, M.I, The vibration of two-dimensional imperfect functionally graded (2D-FG) porous rotating nanobeams based on general nonlocal theory. Mech. Syst. Signal Process. 144 (2020).

[22] Pengfei, Y., Weifeng, L., Liming, P., Yaohong, S., and Jinquan, G., The bending and vibration responses of functionally graded piezoelectric nanobeams with dynamic flexoelectric effect, Results in Physics. 28 (2021).

[23] She, G.L., Liu, H.B., and Karami, B, Resonance analysis of composite curved microbeams reinforced with graphene nanoplatelets, Thin-Walled Struct. 160 (2021).

[24] Arash, I., Aria, Timon R., and Michael, I., F. A finite element model for the thermo-elastic analysis of functionally graded porous nanobeams, European Journal of Mechanics - A/Solids. 77 (2019).

[25] Gafour, Y., Hamidi, A., Benahmed, A., Zidour, M., and Bensattalah, T., Porosity-dependent free vibration analysis of FG nanobeam using non-local shear deformation and energy principle, Adv. Nano Res., 8, 1 (2020) pp. 49-58.

[26] Emad, K., N., Bakhy, H., S., and Al-Waily, M., Analytical and numerical free vibration analysis of porous functionally graded materials (FGPMs) sandwich plate using Rayleigh-Ritz method, Archives of Materials Science and Engineering 110, 1 (2021) pp. 27-41.

[27] Emad, K., N., Bakhy, H., S., and Al-Waily, M., Analytical and Numerical Investigation of Free Vibration Behavior for Sandwich Plate with Functionally Graded Porous Metal Core, Pertanika Journal of Science & Technology 29, 3 (2021) pp. 1655-1682.

[28] A., F., Avila, Failure mode investigation of sandwich beams with functionally graded core, Composite Structures. 81, 3 (2007) pp. 323-330.

[29] ASTM D638, "standard test method for tensile properties of plastics", Annual Book of ASTM Standards, American Society of Testing and Materials, West Conshohocken, 2014.

[30] Can, T., Junwei, L., Yang Y. Ye L., Shiping J., Wenfeng H., Effect of process parameters on mechanical properties of 3D printed PLA lattice structures, Composites Part C: Open Access. 3 (2020).

[31] L., Wang, W., M., Gramlich, and D., J., Gardner, Improving the impact strength of Poly(lactic acid) (PLA) in fused layer modeling (FLM), Polymer. 114(2017) pp. 242–248.

[32] ASTM D790 “Standard test methods for flexural properties of unreinforced and reinforced plastics and electrical insulating materials,” ASTM International, West Conshohocken, Pa, United States, 2014.

[33] Emad, K., N., Bakhy, H., S., and Al-Waily, M, Optimization design of vibration characterizations for functionally graded porous metal sandwich plate structure, Materials Today: Proceedings. (2021).

[34] Vinh, P., V., and Huy, L., Q., Finite element analysis of functionally graded sandwich plates with porosity via a new hyperbolic shear deformation theory, Defence Technology. (2021).

[35] Mohamed, O., B., Mohammed, S., Ahmed, H., Hicham, H., Ahmed, A., D., Stéphane P., and Alain B., On the finite element analysis of functionally graded sandwich curved beams via a new refined higher order shear deformation theory, Composite Structures. 279 (2022).

[36] Arndt, F. K., and Lechner, M., D., Polymer Solids and Polymer Melts–Mechanical and Thermomechanical Properties of Polymers, Springer-Verlag Berlin Heidelberg, 6A3 (2014).

[37] M., D., Do, M., T., Tran, and H., C., Truong, Bending analysis of sandwich beam with functionally graded face sheets using various beam theories by meshfree method, ISAS, Kalpa Publications in Engineering. 3 (2020) pp. 139-149.